Hardware-Constrained Signal Processing for mm-Wave LoS MIMO

B. Mamandipoor[1], M. Sawaby[2] , A. Arbabian[2] and U. Madhow[1]

(1) ECE Department, University of California, Santa Barbara, CA, USA
(2) EE Department, Stanford University, Stanford, CA, USA
Emails: {bmamandi, madhow}@ece.ucsb.edu
{msawaby, arbabian}@stanford.edu

Abstract—At high carrier frequencies, spatial multiplexing gains can be obtained even in line of sight (LoS) environments with reasonable node form factors. We investigate design of a LoS MIMO link operating at millimeter (mm) wave frequencies beyond 100 GHz, with 4-fold spatial multiplexing, and bandwidth of 10-20 GHz, with data rates even with relatively small constellations (QPSK) reaching 80-160 Gbps. Even small misalignments lead to frequency selectivity at these bandwidths, and we show that this leads to performance floors for conventional linear space-time equalizers. An alternative approach, which closely couples hardware and signal processing design in utilizing analog delays with subsymbol precision, is shown to eliminate such error floors. By using analog techniques to address frequency selectivity and to perform spatial demultiplexing, this proposed architecture also alleviates the difficulty of analog-to-digital conversion at high sampling rates.

I. Introduction

There have been significant recent advancements in silicon implementation and low-cost packaging in mm-wave frequencies [1], [2], opening up large swathes of spectrum. In addition to the increased number of degrees of freedom in the time-bandwidth plane, the number of spatial degrees of freedom also increases with carrier frequency. For a transmit array of aperture A_T and a receive array of aperture A_R, the number of spatial degrees of freedom for a LoS link of range R at carrier wavelength λ is approximately $\frac{A_T A_R}{(\lambda R)^2}$ (this follows from a straightforward generalization of [3]). This LoS MIMO result is of limited utility for existing wireless systems at 5 GHz or below ($\lambda = 6$ cm or higher) at the link ranges of typical interest: a 50 m link at 5 GHz requires an aperture of $3m^2$ at each end. As a result, spatial multiplexing for existing wireless systems relies on rich scattering setting originally studied in [4], [5]. On the other hand, LoS MIMO at 50 m becomes feasible at 130 GHz, with a required aperture of $0.11m^2$ at each end, corresponding to a array baseline of the order of 30 cm. Coupling the increased bandwidth with the increase in spatial degrees of freedom opens up the possibility of mm-wave "Wireless Fiber" [6].

The feasibility of transmitting multiple independent data streams through spatial multiplexing in LoS environments has been studied [3] and demonstrated through hardware prototypes [7], [8]. Many authors have also investigated the capacity of LoS MIMO channel and identified the optimal array geometries that maximize the capacity [9], [10]. The required geometrical constraints are also related to the Rayleigh criterion from diffraction limited optics [11]. Our focus in this paper is on transceiver design for pushing the limits of LoS MIMO in terms of bandwidth and carrier frequency, accounting for hardware constraints and imperfections.

Nominal system: We consider a nominal LoS MIMO link operating at carrier frequency $f_c = 130$ GHz, with 4-fold spatial multiplexing. The bandwidth is 20 GHz, which holds the potential for data rate of 20Gbps/real dimension with QPSK modulation (overall data rate of 160 Gbps). The nominal range between Tx and Rx arrays is set to $R = 100$m.

Misalignment: A key design focus is on link misalignment, which introduces significant channel memory at the high bandwidths of interest. For instance, if the spacing between two array elements $d \approx 34$ cm, then 7.5 degree misalignment introduces about 3 symbol memory at 20 Gsamples/s. While misalignment should be minimized at installation, transceiver design must allow for imperfections. This is an even more critical issue when using a reflector to sidestep LoS blockage (see Figure 1), where direct visual access is not available between the link endpoints.
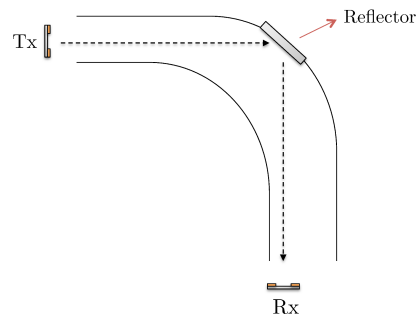

Fig. 1: Side-stepping LoS blockage using a reflector

ADC bottleneck: Another fundamental bottleneck at high bandwidths is analog-to-digital conversion [12], [13]. The increased dynamic range due to spatial multiplexing makes discretization prior to digital signal processing particularly challenging.

In this paper, we show that, even if we ignore the ADC bottleneck, conventional linear space-time techniques for equal-

ization and spatial demultiplexing leads to performance floors. We therefore propose a fundamentally new analog-centric architecture, which uses analog delays with subsymbol precision to appropriately shape the space-time channel, together with an analog channel separation network. We show that this approach eliminates the performance floor, while also reducing the dynamic range of the signals to be ultimately discretized.

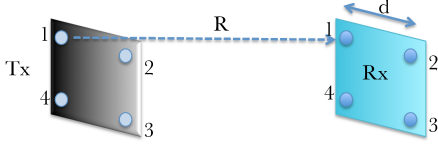## II. RAYLEIGH CRITERION FOR ALIGNED CHANNEL

Fig. 2: Nominal channel with aligned arrays

We first review the geometry of an aligned LoS MIMO link. The transmitter (Tx) and receiver (Rx) each employs a 4-element square array with elements located at the corners. We assume that the elements are highly directive, so that reflections can be ignored. The arrays are aligned broadside and separated by distance R. The received signal is given by

$$\bar{y} = \tilde{H}\bar{s} + \bar{z},$$

where $\tilde{H} \in \mathbb{C}^{N \times N}$ is the aligned channel matrix, $\bar{s} \in \mathbb{C}^{N \times 1}$ denotes the vector of transmitted symbols, and $\bar{z} \sim CN(\mathbf{0}, 2\sigma^2 \mathbb{I}_N)$ is additive white Gaussian noise. Ignoring path loss differences among Tx-Rx antenna pairs, the complex channel gain from the mth transmitter element to the nth receiver element is given by

$$\tilde{h}_{mn} = e^{-j\frac{2\pi}{\lambda}p_{m,n}}, \tag{1}$$

where λ is the carrier wavelength, and $p_{m,n}$ is the path length between the elements [3]. When R is much larger than the size of either array, we can approximate the path length by $p_{m,n} \approx R + \zeta_{m,n}^2/(2R)$, where $\zeta_{m,n}$ is the distance in the cross-range plane (e.g $\zeta_{1,1} = 0$, $\zeta_{1,3} = \sqrt{2}d$, and so on). The normalized channel matrix for a 4×4 MIMO system can be written as

$$\tilde{H} = \frac{1}{2} \begin{bmatrix} 1 & e^{-j\phi} & e^{-j2\phi} & e^{-j\phi} \\ e^{-j\phi} & 1 & e^{-j\phi} & e^{-j2\phi} \\ e^{-j2\phi} & e^{-j\phi} & 1 & e^{-j\phi} \\ e^{-j\phi} & e^{-j2\phi} & e^{-j\phi} & 1 \end{bmatrix}, \tag{2}$$

where $\phi \approx \frac{\pi d^2}{\lambda R}$. It is easy to see that for $\tilde{H}$ to be unitary, we should have $\phi = k\frac{\pi}{2}$ for some $k \in \{2l + 1 : l \in \mathbb{Z}^+\}$. Setting $k = 1$ gives the minimum acceptable inter-element spacing as a function of range and wavelength, $d_{\min} = \sqrt{\frac{R\lambda}{2}}$. For our nominal system parameters, we have $d_{\min} \approx 34cm$.

III. MISALIGNED CHANNEL MODEL

We now include misalignment in the channel model. As shown in Figure 3, the misaligned channel is a concatenation of three parts; Tx misalignment, the ideal channel, and the Rx

misalignment. We can approximate the effect of misalignment by adding *delays* in the complex baseband representation of the channel. This approximation allows us to decompose the channel as $H \approx T_{rx}\tilde{H}T_{tx}$, where T_{tx} and T_{rx} are diagonal matrices that contain the information about corresponding Tx and Rx delays. For instance, i^{th} diagonal element of T_{tx} can be expressed as $z^{-\mu_i}$, indicating a delay of μ_i for i^{th} Tx element.

One can also decompose the misalignment matrices, e.g. T_{tx}, further into multiples of symbol-period delay and fractional delay matrices, denoted by $T_{n,tx}$ and $T_{\epsilon,tx}$, respectively. Therefore, full-channel decomposition can be expressed as

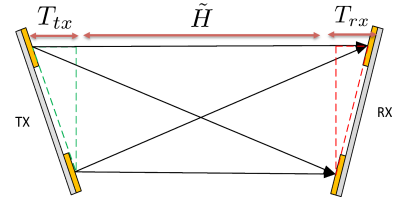$$H = T_{\epsilon,rx}T_{n,rx}\tilde{H}T_{\epsilon,tx}T_{n,tx}. \tag{3}$$

Fig. 3: misalignment

We can now derive the time domain channel impulse response from m^{th} transmitter to the nth receiver, denoted by $h_{mn}(t)$. Let μ_m and τ_n represent the delays corresponding to the Tx and Rx elements, respectively. Assuming a Nyquist pulse $p(t)$, we have

$$h_{mn}(t) = \alpha_{mn}p(t - \mu_m - \tau_n), \tag{4}$$

where $\alpha_{mn} = \tilde{h}_{mn}\exp(-j2\pi f_c(\mu_m + \tau_n))$. Sampling at the symbol rate, the discrete-time channel is given by $h_{mn}[k] = \alpha_{mn}p(kT - \mu_m - \tau_n)$. The overall L-tap MIMO channel in the matrix form is given by

$$H[k] = \sum_{l=0}^{L-1} H_l\delta(k - l), \tag{5}$$

where $H_l \in \mathbb{C}^{N \times N}$ contains the channel coefficients $h_{mn}[l]$, $m, n \in \{1, 2, \ldots, N\}$. Let $\bar{s}[k] = [s_1[k], s_2[k], \ldots, s_N[k]]^T$ be the transmitted vector at time k. The received vector can be expressed as

$$\bar{y}[k] = \sum_{l=0}^{L-1} H_l\bar{s}[k - l] + \bar{z}[k], \tag{6}$$

with $\bar{z}[k]$ containing the noise samples.

Oversampling: The aligned channel in (2) is full-rank and memoryless, hence channel separation is simply carried out by applying a single-tap spatial filter $\tilde{H}^{-1}$. On the other hand, the misaligned channel in (5) is frequency-selective, hence linear inversion requires fractionally spaced sampling. However, due to the difficulty of ADC at the bandwidths of interest, we restrict attention to symbol rate sampling for both our benchmark digital scheme and our analog-centric architecture. The use of multiple receivers, and the variation of the channels

from a given transmitter to the different receivers, does provide an effect similar to oversampling, but the available degrees of freedom must be used for both spatial demultiplexing and equalization in the presence of misalignment.

IV. BENCHMARK: SPACE-TIME MMSE EQUALIZER

For our benchmark, we consider conventional space-time linear processing, with N finite-impulse-response (FIR) filters followed by hard decisions. Consider a time window of size W samples at the Rx output, and stack the observations in a vector defined by

$$\mathbf{y} = \left[\bar{y}^T[k], \bar{y}^T[k-1], \ldots, \bar{y}^T[k-W+1]\right]^T, \quad (7)$$

where $(\cdot)^T$ denotes transposition. It is easy to see that

$$\mathbf{y} = \mathbf{U}\mathbf{s} + \eta, \quad (8)$$

where $\mathbf{U} \in \mathbb{C}^{WN \times N(L+W-1)}$ is a block Toeplitz matrix of channel coefficients,

$$\mathbf{U} = \begin{bmatrix} H_0 & H_1 & \ldots & 0 & 0 \\ 0 & H_0 & H_1 & \ldots & 0 \\ \vdots & & & & \\ 0 & 0 & \ldots & H_{L-2} & H_{L-1} \end{bmatrix}, \quad (9)$$

and $\mathbf{s} = \left[\bar{s}^T[k], \bar{s}^T[k-1], \ldots, \bar{s}^T[k-L-W+1]\right]^T$ is the vector of all transmitted symbols with a nonzero response in the observation interval [14]. We assume additive Gaussian noise, white across time and space, $\eta \sim CN(0, 2\sigma^2 \mathbb{I}_{NW})$. All symbols in $\mathbf{s}$ corresponding to the index set $\Gamma_t = \{iN + t : i \in \{0, 1, \ldots, L+W-1\}\}$ are sent from t^{th} transmitter. Among these symbols we identify a desired symbol $\mathbf{s}[\gamma_t]$ by $\gamma_t \triangleq \arg\max_{j \in \Gamma_t} ||u_j||_2$, where u_j is the jth column of $\mathbf{U}$. The MMSE correlator for $\mathbf{s}[\gamma_t]$ is defined by

$$c_{\gamma_t} = \arg\min_{c \in \mathbb{C}^{N \times 1}} \mathbb{E}[|c^H \mathbf{y} - \mathbf{s}[\gamma_t]|^2]. \quad (10)$$

We obtain the standard solution [15] $c_{\gamma_t} = (\mathbf{U}\mathbf{U}^H + \frac{1}{\rho}\mathbb{I})^{-1} u_{\gamma_t}$, where $\rho = \frac{\sigma_s^2}{2\sigma^2}$ is the SNR for hypothetical single-input single-output (SISO) system with unit norm channel gain, and σ_s^2 is the average signal power. The signal to interference and noise ratio (SINR) at the output of the equalizer for t^{th} stream is given by

$$\text{SINR}_t = \frac{|\langle c_{\gamma_t}, u_{\gamma_t}\rangle|^2}{\sum_{i \neq \gamma_t} |\langle c_{\gamma_t}, u_i\rangle|^2 + \frac{1}{\rho}||c_{\gamma_t}||_2^2}. \quad (11)$$

For our simulations, we consider QPSK with raised cosine pulse $p(t)$ with roll-off factor 0.25. The delays are independent and identically distributed uniform random variables $\mu_i, \tau_j \sim$ Uniform$[0, 150) \times 10^{-12}$ seconds. The equalizer time window $W = 5$ samples. Figure 4 shows the output SINR averaged over 4 streams and multiple channel realizations. We see a rather clear separation between noise-limited and interference-limited regimes. SINR in the noise-limited regime is near-optimal and insensitive to the channel realization, whereas in the interference-limited regime, SINR is sensitive to the channel realization, and exhibits a plateau.
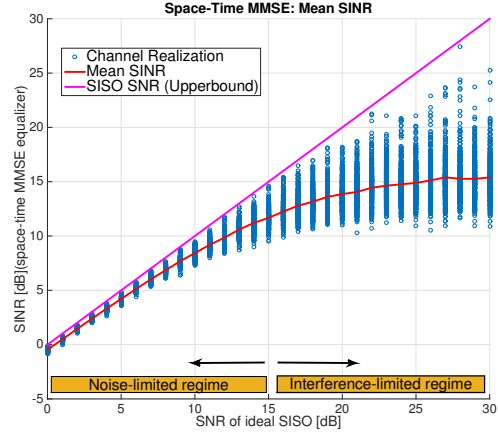

Fig. 4: Average SINR at the output of MMSE equalizer.

A. Fractional Analog Delays

In order to motivate our analog-centric architecture, we first explore whether poor channel realizations can be reshaped by inserting fractional analog delays at the Tx or Rx. Figure 5 shows the performance of the equalizer in terms of symbol error rate (SER) and SINR for a bad channel realization. Performance floors for two of the streams are evident from both the symbol error rate and SINR curves.

Next, we modify the system architecture by inserting fractional analog delays as depicted in Figure 6. Figure 7 shows the result of adding 20 and 30 psec delays at transmit elements 3 and 4, respectively. We can see that the error floors in SER have been eliminated, and that the performance is close to that of ideal ISI-free QPSK.

The preceding example clearly shows the potential of employing analog delays, and motivates the architecture discussed in the next section.

V. HARDWARE-OPTIMIZED MIMO PROCESSING

The conventional all-digital architecture that we considered in Section IV, requires high-precision ADCs sampling at the symbol rate. If we want to use drastically low-precision ADCs not only we expect a degradation in the performance of the space-time equalizer, but also the effect of adding fractional delays vanishes. We therefore propose a fundamentally new architecture based on information-preserving analog processing, as opposed to early digitization.

Figure 8 shows an analog-centric architecture which achieves two objectives: it uses analog delays for channel reshaping, and it uses an analog channel separation network (CSN). Thus, the role of full-bandwidth ADC is reduced to that of performing hard decisions after the CSN: for QPSK, this amounts to sign detection for I and Q, assuming that carrier synchronization is achieved by other means. Of course, choosing the analog delays and setting the CSN coefficients requires DSP, but this is carried out based on samples acquired at a much slower rate.
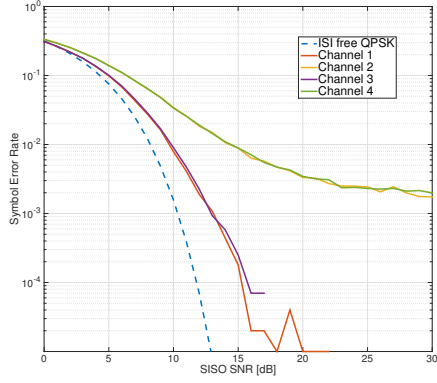
(a) Symbol error rate
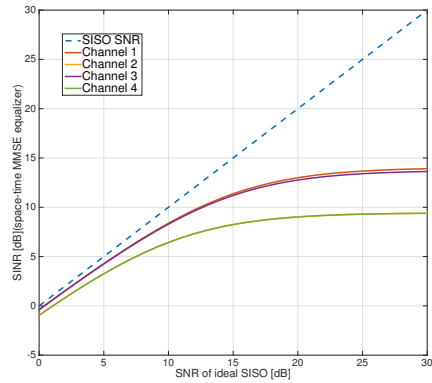
(b) SINR
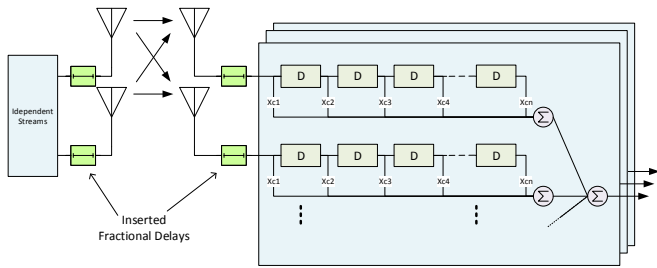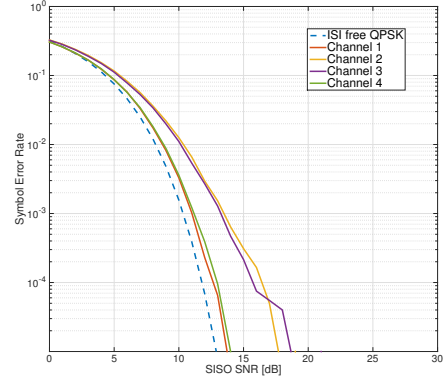
Fig. 5: Equalizer performance: bad channel realization

(a) Symbol error rate

(b) SINR

Fig. 7: Equalizer performance after inserting the delays

Fig. 6: Analog fractional delays followed by digital space-time equalizer.
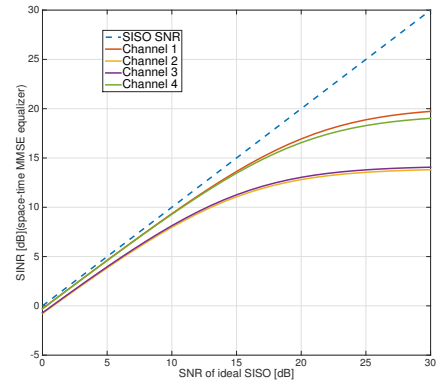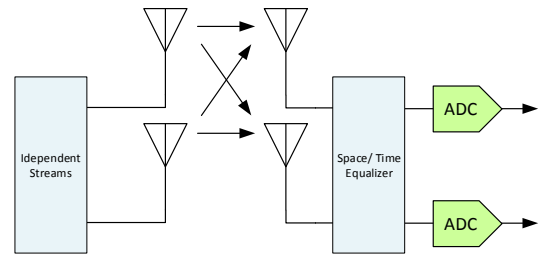

Fig. 8: Analog processing to relax ADC requirement

A. Analog Channel Separation Network (CSN)

Our proposed system architecture is based on the channel model that we have developed in Section III (Figure 9). Assuming independent data streams sent from different Tx elements, full symbol delays at the Tx are irrelevant (i.e., we can ignore $T_{n,tx}$), so that we only need to consider fractional delays, $T_{\epsilon,tx}$, in modeling the Tx. Thus, the goal of our design is to perform the following high-level "inversion":

$$\hat{y} = T_{\epsilon,tx}^{-1} \tilde{H}^{-1} T_{rx}^{-1} \ T_{rx} \tilde{H} T_{tx} \ \bar{s}. \tag{12}$$

In order to eliminate the effect of Rx misalignment, we employ digitally-controlled analog delay-lines at each Rx chain (T_{rx}^{-1}). These analog modules provide the flexibility of adding up to several symbol period delay with sub-symbol precision, in order to emulate a perfectly aligned Rx array. The next step is to separate the streams by applying a single-tap spatial equalizer ($\tilde{H}^{-1}$), implemented using complex multiply-and-add operations in the analog domain. Finally, we need to account for the fractional delays at the Tx side, by inserting sub-symbol delays ($T_{\epsilon,tx}^{-1}$), at the output of the single-tap matrix demultiplexer.

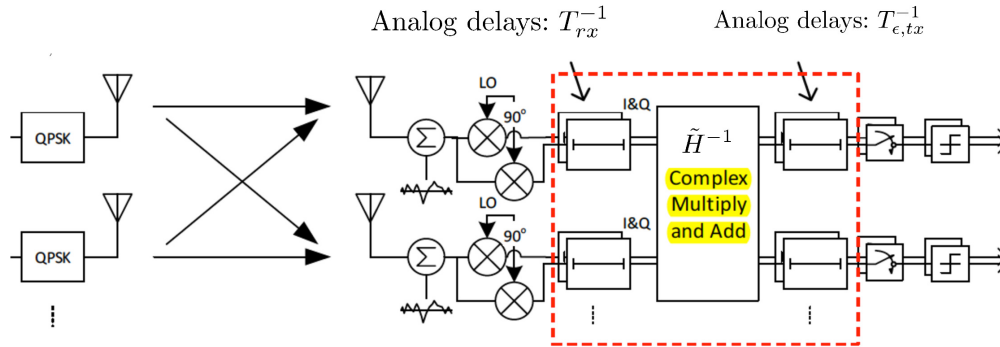We consider two scenarios for evaluating the performance

Fig. 9: Analog channel separation network.

of the analog CSN, (1) allowing the delay durations and gain values to take values within a certain range with infinite precision, (2) restricting the possible values for delays and gains to a finite set. For the second scenario, we consider uniformly spaced delay values up to 150 psec, with 15 psec steps. The complex gains in the single-tap spatial equalizer are assumed to have a maximum 1dB error in magnitude and quantized phase with 20 degrees step size. As shown in Figure 10, the analog CSN with infinite precision parameters achieves the symbol error rate of an ideal ISI free QPSK. Moreover, restricting the parameters to take values in a finite set, leads to an SNR penalty (which is about $1 - 2$ dB, depending on the target SER), but more importantly, no error floor appears for any of the streams.
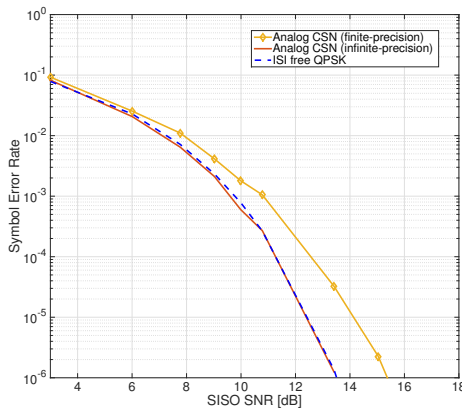

Fig. 10: Analog CSN performance.

VI. Conclusion

By taking advantage of the specific nature of the channel impairment due to misalignment, our proposed analog-centric architecture is able to eliminate performance floors while alleviating ADC requirements. Ongoing work focuses on hardware prototyping and algorithm development aimed at demonstrating ultra high-speed LoS MIMO above 100 GHz.

References

[1] B. Gaucher et al., "Silicon germanium based millimetre-wave ICs for Gbps wireless communications and radar systems," Semiconductor Science and Technol., vol. 22, no. 1, p. S236, 2007.

[2] M. Tabesh, C. Jiashu, C. Marcu, K. Lingkai, K. Shinwon, A. M. Niknejad, E. Alon, "A 65 nm CMOS 4-Element Sub-34 mW/Element 60 GHz Phased-Array Transceiver," in Solid-State Circuits, IEEE Journal of , vol.46, no.12, pp.3018-3032, Dec. 2011.

[3] E. Torkildson, U. Madhow, and M. Rodwell, "Indoor Millimeter Wave MIMO: Feasibility and Performance," in Wireless Communications, IEEE Transactions on , vol.10, no.12, pp.4150-4160, December 2011.

[4] G. Foschini and M. Gans, "On Limits of Wireless Communication in a Fading Environment when using Multiple Antennas," Wirel. Pers. Commun., vol. 6, no. 3, pp. 311-335, 1998.

[5] E. Telatar, "Capacity of Multi-antenna Gaussian Channels," European Transactions on Telecommunications, Vol. 10, No. 6, pp. 585-595, Nov/Dec 1999.

[6] E. Torkildson, B. Ananthasubramaniam, U. Madhow, and M. Rodwell, "Millimeter-wave MIMO: wireless links at optical speeds," in Proc. of 44th Allerton Conference on Communication, Control and Computing, Sep. 2006.

[7] C. Sheldon, M. Seo, E. Torkildson, M. Rodwell, and U. Madhow, "A 2.4 Gb/s millimeter-wave link using adaptive spatial multiplexing," IEEE Int. AP-S Symp., July 2010.

[8] —-, "Four-channel spatial multiplexing over a millimeter-wave line-of-sight link," IEEE - MTTS International Microwave Symposium, June 2009.

[9] P. Larsson, "Lattice array receiver and sender for spatially orthonormal MIMO communication," in Proc. IEEE 61st Vehicular Tech. Conf., vol. 1, pp. 192-196, May 2005.

[10] F. Bohagen, P. Orten, and G. Oien, "Design of optimal high-rank line-of- sight MIMO channels," IEEE Trans. Wireless Commun, vol. 6, no. 4, pp. 14201425, Apr. 2007.

[11] A. Thaning, P. Martinsson, M. Karelin, and A. T. Friberg, "Limits of diffractive optics by communication modes," J. Optics A: Pure and Applied Optics, vol. 5, no. 3, p. 153, 2003.

[12] R. H. Walden, "Analog-to-digital converter survey and analysis," IEEE J. Sel. Areas Commun., vol. 17, no. 4, pp. 539-550, April 1999.

[13] B. Murmann, "Energy limits in a/d converters," Faible Tension Faible Consommation (FTFC), 2013 IEEE, 2013.

[14] A. Voulgarelis, M. Joham, W. Utschick, "Space-time equalization based on V-BLAST and DFE for frequency selective MIMO channels," in Acoustics, Speech, and Signal Processing, 2003. Proceedings. (ICASSP '03). 2003 IEEE International Conference on , vol.4, no., pp.IV-381-4 vol.4, 6-10 April 2003.

[15] U. Madhow, Fundamentals of Digital Communication, 2008 :Cambridge Univ. Press.